THE ASTROPHYSICAL JOURNAL, 383:511–523, 1991 December 20


# NEW PHOTOIONIZATION MODELS OF INTERGALACTIC CLOUDS

MEGAN DONAHUE[1,2,3] AND J. MICHAEL SHULL[1,2]

*Received 1990 August 17; accepted 1991 July 1*

## ABSTRACT

We present new photoionization models of optically thin, low-density intergalactic gas at constant pressure, photoionized by QSOs. To improve accuracy of ionization calculations, our code uses Opacity Project photoionization cross sections for the ground states of C, N, O, and Si and makes approximate corrections for the radiative recombination rates using detailed balance. We model all ion stages of H, He, C, N, O, Si, and Fe, plus $H_2$ and predict the column density ratios of clouds at specified values of ionization parameter $U = n_\gamma/n_H$ and cloud metallicity. For gas photoionized by quasars, a two-phase (cloud-intercloud) medium cannot exist at $T = (1–3) \times 10^4$ K, so that pressure confinement of the Ly$\alpha$ clouds is problematic.

We derive new metallicity limits for absorption systems at $z = 3.321$ (S5 0014+81) and at $z = 2.9676$ (PKS 2126−158). In addition, we find a stable molecular phase in Ly$\alpha$ clouds, with $U \approx 10^{-7}$ to $10^{-5}$ and $n(H_2)/n(H\ I) \approx 10^{-2}$, in which molecular cooling produces $T < 10^4$ K, as suggested by recent line width data. Photoelectron escape from low-column H I clouds can reduce the heating and explain the observed narrow line widths. If the ionizing radiation flux $J_0 = 4\pi I_0 \approx 10^{-21}$ ergs cm$^{-2}$ s$^{-1}$ Hz$^{-1}$, as inferred for several absorption systems in QSO 2206−199N, these $10^4$ K clouds require high densities ($n_H \approx 0.1$ cm$^{-3}$) and have significant neutral fractions. The inferred cloud thicknesses are $10^{5–9}$ times smaller than the lateral extents estimated by double-QSO observations. Such aspect ratios are difficult to understand, and the large pressures would make the sheet like clouds difficult to confine by means other than ram pressure. The value of $U$ required to explain the H I line widths is also much smaller than that needed to explain the observed ratios $N(C\ IV)/N(C\ II) \geq 1$ in sharp metal-line systems.

*Subject headings:* atomic processes — intergalactic medium — molecular processes — quasars

## 1. INTRODUCTION

The absorption lines in QSO spectra due to intergalactic hydrogen clouds are one of the most sensitive indicators of the distribution of matter and ionizing radiation at high redshift. The increasing sensitivity and resolution of astronomical instruments may soon allow observers to measure the ionizing flux incident on the clouds and to estimate cloud properties such as metallicity, temperature, and density. Recent observations (Pettini et al. 1990) of optically thin Ly$\alpha$ absorption lines suggest that some clouds have lower temperatures (5000 – 10,000 K) than previously supposed. If the clouds are indeed this cool, their inferred densities are much higher and their sizes and masses are much smaller than in the conventional view (see review by Sargent & Steidel 1990).

Steidel & Sargent (1989) have used observations of metal-line systems to estimate the shape of the ionizing background at high redshift; others (Chaffee et al. 1985, 1986; Bechtold et al. 1987) have observed metal-line systems to constrain the metallicity in the clouds. The intergalactic cloud photoionization model presented here includes a sample of metals (C, N, O, Si, and Fe) and a range of metallicities in order to provide observers with diagnostic tools to investigate the physical characteristics and environment of these clouds.

Photoionization models rely on the atomic data provided by major efforts such as the Opacity Project (Seaton 1987; Pradhan 1988). For some ions, the new ground-state cross sections are larger than earlier values, especially at higher energies. To apply these new cross sections semiconsistently, we have made an approximate correction to the radiative recombination rates, applying the Milne relation of detailed balance to the ground-state photoionization cross sections and scaling the excited states accordingly. A full calculation of the radiative recombination rates must await the dissemination of the excited-state cross sections; for many ions the recombination at $T \geq 10^4$ K is dominated by dielectronic recombination, whose rates are still uncertain. We also include ion charge exchange with H I and pay special attention to the effects of high-energy photons, such as Auger electrons and Compton heating. Our models predict an ionization level somewhat higher than that predicted by earlier models with similar spectral shapes and ionization parameters. However, until radiative and dielectronic recombination rate coefficients are computed to the same accuracy as the photoionization cross sections, all conclusions about the ionization remain uncertain.

In § 2 we describe our model and its assumptions. In §§ 3 and 4 we present the results of model runs and discuss the consequences of these results for cloud temperature, metallicity, and geometry. Molecular cooling and photoelectron escape may help explain the low temperatures inferred by Pettini et al. (1990), although the required cloud pressures are high and the cloud aspect ratios are extremely large. In the Appendix we present a calculation of Fe photoionization equilibrium that extends the previous work of Weisheit (1974) on the modification by Auger transitions. In § 5 we summarize our conclusions and discuss some possibilities for future work.

[1] Joint Institute for Laboratory Astrophysics, University of Colorado and National Institute of Standards and Technology, Campus Box 440, Boulder, CO 80309-0440.

[2] Center for Astrophysics and Space Astronomy, Department of Astrophysical, Planetary, and Atmospheric Sciences, University of Colorado.

[3] Postal address: Observatories of the Carnegie Institution of Washington, 813 Santa Barbara Street, Pasadena CA 91101.

## 2. THE PHOTOIONIZATION MODEL

### 2.1. *Ionization Equilibrium*

In our model, we assume that the gas is tenuous and optically thin in the Lyman continuum. Therefore collisional ionization is not important in determining the ionization structure of the gas, although we do include it self-consistently. We also ignore radiative transfer; previous photoionization models (e.g., Bergeron & Stasinka 1986) showed that optical depth in the Lyman continuum does not affect the results until $N(\mathrm{H\ I}) \gtrsim 10^{17.3}\ \mathrm{cm}^{-2}$. Because we do not account for quenching of collisionally excited lines, our models are valid only for $n_{\mathrm{H}} \lesssim 100\ \mathrm{cm}^{-3}$. We do allow a trace population of $H_2$ molecules to form via the $H^-$ catalytic process; the $H_2^+$ catalytic process is somewhat less important.

The model requires an input photoionizing spectrum, which we nominally model after the form for a typical QSO given by Mathews & Ferland (1987, hereafter MF). In this spectrum, the specific energy flux varies as $\nu^{-\alpha}$, where $\alpha$ steepens from 0.5 (13.6–23.7 eV) to 1.0 (23.7–56.2 eV) to 3.0 (56.2–365 eV), and then flattens to $\nu^{-0.7}$ between 365 eV and $10^5$ eV. In order to compare our work with previous efforts, we also test a $f_\nu \propto \nu^{-1.5}$ shape in the ionizing continuum. This is probably a fair approximation for the shape of the ionizing background since redshift effects do not appear to dominate (Bajtlik, Duncan, & Ostriker 1988). In practice, we do not find dramatic differences in our results due to differences in the assumed shape of the QSO input spectra.

We need to clarify our definitions of radiation fluxes and specific intensity, since there has been occasional confusion about these terms. We define $J_0$ as the specific flux at 13.6 eV in units of ergs $\mathrm{cm}^{-2}\ \mathrm{s}^{-1}\ \mathrm{Hz}^{-1}$. This is to be contrasted with $I_0$, the specific intensity at 13.6 eV in units of ergs $\mathrm{cm}^{-2}\ \mathrm{s}^{-1}\ \mathrm{Hz}^{-1}\ \mathrm{sr}^{-1}$, where $J_0 = 4\pi I_0$ for isotropic radiation fields. To describe the thermal and ionization state of the gas, we adopt the dimensionless "ionization parameter," $U = n_\gamma/n_{\mathrm{H}}$, equal to the ratio of the density of ionizing photons to the total hydrogen density. We can convert between $U$ and the ratio $J_0/n_{\mathrm{H}}$ for a given spectal shape through a multiplicative factor $M$ such that $U = M(J_0/n_{\mathrm{H}})$. For the spectra discussed here, $M$ (in cgs units) is $5.19 \times 10^{15}$ and $3.36 \times 10^{15}$ for MF and $\nu^{-1.5}$ spectra respectively.

The valence-shell, ground-state photoionization cross sections of all ions of C, N, and O, plus Si III and Si IV, were provided by the collaborative effort known as the Opacity Project, involving atomic physicists in Belfast, Boulder, Caracas, London, Münich, Paris, and Urbana. Cross sections for Fe and for Si V and higher came from Reilman & Manson (1978); those for Si I and Si II came from Chapman & Henry (1972). The Opacity Project provides calculations of atomic energy levels, oscillator strengths, and photoionization cross sections for all atoms and ions of astrophysically abundant elements. A general description of this project and specific calculations and applications are given in a series of 11 papers in the Journal of Physics B (1987–1989) entitled Atomic Data for Opacity Calculations, denoted ADOC I-XI. The reader is referred particularly to ADOC I (Seaton 1987) for an overview; for specific photoionization cross sections see ADOC IV (Yu & Seaton 1987–C II); ADOC VII (Fernley, Taylor, & Seaton 1987–He-like ions); ADOC IX (Peach, Saraph, & Seaton 1988–Li-like ions); ADOC X (Luo et al. 1989–O III); and ADOC XI (Luo & Pradhan 1989–other C-like ions). These new data are computed for a number of energies above threshold, with sufficient resolution to treat the numerous autoionizing resonances.

For many ions, the ground-state photoionization cross sections from the Opacity Project are higher than previous computations summarized by Osterbrock (1989), and they do not drop off as quickly with energy. Threshold cross sections for the carbon isosequence were substantially increased, by factors of 1.45, 1.17, and 1.23 for C I, N II, and O III, respectively. For other ions of C, N, and O, the changes at threshold were less than 10%. For the interstellar and intergalactic applications of our photoionization models, we may assume that all atoms and ions are in their ground states. Since most intergalactic clouds are optically thin in the H I Lyman continuum, they are also optically thin to photoionization of heavy elements, even with the increased cross sections in the autoionizing resonances.

Because the Opacity Project computed cross sections to only about a factor of 4 above threshold, these data do not apply to X-ray ionization. In order to extrapolate the Opacity Project cross sections to higher energies, we used fits of the cross sections to the standard two power-law form,

$$\sigma(E) = \sigma_0\left[\alpha\left(\frac{E_T}{E}\right)^s + (1-\alpha)\left(\frac{E_T}{E}\right)^{s+1}\right], \quad (1)$$

where $E_T$ is the threshold energy. Since our input spectra are fairly steep, the high-energy portions of the spectra do not contribute substantially ($\lesssim$ 1%–10%) to photoelectric heating of the ions. However, the uncertainties in the cross sections at 1–10 keV limit the precision of our code when applied to harder X-ray spectra.

The rates of photoionization and photoelectric heating were derived from the computed cross sections and their extrapolations. It should be noted that because the input ionizing spectra are broad-band, whereas resonances in the ground-state photoionization cross sections are narrow, it is a good approximation to average across the narrow resonances. This is not true for the broad resonance structure that occurs in the PEC (photoexcitation of core) resonances of some excited states and for the ground states of several atoms and ions. For the low densities in the intergalactic or interstellar medium, photoionization occurs predominantly from the ground states, for which we use the accurate cross sections.

For the X-ray photoionization of the K and L subshells of C, N, O, and Si we used fits reported in Daltabuit & Cox (1972). For iron we used Reilman & Manson (1978), digitizing their plots and fitting the results to the two power-law formula; the cross sections from 2*s* states of Fe were decreased by a factor of 10, owing to an error in their Figure 2. We were not able to fit the ions of Fe I (4*s*, 3*p*, 3*d* subshells), Fe II (4*s*, 3*p*, 3*d*), Fe III (3*p*, 3*d*), Fe IV (3*p*, 3*d*), Fe IV (3*p*, 3*d*), and Fe V (3*d*). For these ions we numerically integrated the photoionization rates and photoionization heating rates with a Runge-Kutta fourth–fifth order integration scheme.

For Auger and fluorescent transitions following inner-shell ionization in C, N, O, and Si, we used the formalism for effective ionization rates in Weisheit (1974) and Weisheit & Dalgarno (1972). For Fe, we extended the Weisheit formalism (see the Appendix) using the probabilities for Auger emission computed by Jacobs & Rozsnyai (1986). For heating by Auger electrons except for Fe, we use the tabulations of Shull (1979) and Shull & Van Steenberg (1985). The iron K-shell fluorescent yields range from 31% (Fe I) to 49% (Fe XXII), while Fe XXIII (11%—see Chen et al. 1981) and Fe XXIV (75% into Kα photon

and 25% into a two-photon transition) are special cases. These radiative transitions are included in our treatment of the Auger cascade (Jacobs & Rozsnyai 1986). The Fe Auger heating is approximated by calculating the average amount of energy given to the Auger electrons for every primary photoionization. Because the plasma is usually highly ionized, most of the heat is carried in the Auger electrons expelled from the L-shell by K-shell photoionization. These K-shell ionizations therefore dominate the high-temperature Auger heating by iron. However, the heating of intergalactic clouds at $T \approx 10^4$–$10^5$ K is dominated by H I, He I, He II, and ions of carbon and oxygen.

The recombination coefficients (radiative plus dielectronic) we obtain from Woods, Shull, & Sarazin (1981), Shull & Van Steenberg (1983), and Arnaud & Rothenflug (1985), with corrections for the new photoionization data using the Milne relation of detailed balance (Osterbrock 1989). Since we we do not yet have access to photoionization cross sections from all excited states, we corrected the radiative recombination rate coefficients by assuming that the changes in the ground state cross section were characteristic of the excited states. The changes were substantial only for ions in the carbon isosequence (C I, N II, O III). A fully consistent set of radiative recombination rates can be incorporated once the excited-state photoionization cross sections are available from the Opacity Project. At low temperatures, we include dielectronic recombination rate coefficients from Nussbaumer & Storey (1983) and, for recombination to O IV, from Badnell (1988).

One of the other features of our code is a careful inclusion in our ionization balance equations of charge exchange processes between metal ions and H°. We assumed that $O^+ + H^\circ \rightarrow O^\circ + H^+ + 0.02$ eV is a very fast resonant reaction (Field & Steigman 1971) and thus $n(O^+)/n(O^\circ) = (8/9)n(H^+)/n(H^\circ)$. We also include the inverse ionizing reaction to $Si^{+2} + H^\circ \rightarrow Si^+ + H^+ + 2.74$ eV (Baliunas & Butler 1980) since it is also a near-resonant process to the Si II ground state. For the rate coefficients for $Si^{+2} + H^\circ$ we use a fit to the calculations of McCarroll & Valiron (1976). For the inverse (ionizing) reaction we use $k_{up} = (k_{down}/3) \exp(-2.74 \text{ eV}/kT)$. All other metal ions are assumed to charge-transfer into excited states and thus are not resonant reactions. These rate coefficients are usually large ($\sim 10^{-9}$ cm$^3$ s$^{-1}$) for collisions of H° with triply ionized species and with several doubly ionized species (N III, O III, Si III) and were obtained from compilations of Butler & Dalgarno (1979, 1980), Butler, Heil, & Dalgarno (1980), and Dalgarno, Heil, & Butler (1981). Owing to a lack of quantal calculations for Fe ions, we adopt a conservative approach and assume low charge transfer rate coefficients ($10^{-12}$ cm$^3$ s$^{-1}$) to Fe I and Fe II, and relatively large rate coefficients ($10^{-9}$ cm$^3$ s$^{-1}$) to higher Fe ion stages.

### 2.2. *Thermal Equilibrium*

In the energy balance, we include the physical processes of photoelectric heating, Compton heating and cooling, collisional ionization, collisional line excitation (H, He, C, N, O, Si, and Fe), recombination (dielectronic and radiative) cooling, and thermal bremsstrahlung. For collisional line excitation we calculate emissivities for 117 lines of Fe II–Fe XXVI (Gaetz & Salpeter 1983; fine-structure lines from M. Shull [private tabulations]), eight hydrogen lines, 19 helium lines, 35 C lines (including three fine-structure lines of C I and C II excited by collisions by neutral hydrogen as well as by electrons and two lines excited by ionized hydrogen), 26 N lines, and 35 O lines (including two fine-structure lines of O I excited by neutral hydrogen). Collisional ionization rates were obtained from Shull & Van Steenberg (1982).

We make the approximation that all the energy of the ejected photoelectron is deposited into the gas as heat. As the neutral fraction of the gas increases, a higher fraction of this energy is deposited into ionization and excitation of neutral hydrogen. However, this fraction is a strong function of the energy of the photoelectron. For the principal heating contributions at high neutral fraction (photoionization of H, He, and C), the average energies of the valence-shell photoelectrons are 10–30 eV, and thus nearly all of their energy is deposited as heat (Shull & Van Steenberg 1985). Therefore this approximation is justified in the case where the electron column density is sufficient for the electron to deposit its energy via Coulomb collisions. This may not be justified if the clouds are extremely thin, $d < 10^{13}$ cm or so. In § 4.3 we discuss the consequences of the partial loss of heat through photoelectron escape.

Since the relevant temperatures are substantially lower than relativistic, we can approximate the photon cross section of the electron for Compton heating and cooling with a Klein-Nishina cross section (Rybicki & Lightman 1979). The difference between the Compton heating and cooling rate (ergs s$^{-1}$ cm$^{-3}$) can thus be expressed as

$$H_{\text{comp}} - C_{\text{comp}} = n_e \int_{E_{\text{low}}}^{E_{\text{high}}} \mathscr{F}_E (E - 4kT) \frac{\sigma(E)}{m_e c^2} \, dE \,, \qquad (2)$$

where $\mathscr{F}_E$ is the photon energy flux and $\sigma(E)$ is the Klein-Nishina cross section.

### 2.3. *Molecular Physics*

We calculate the molecular hydrogen content of the gas by assuming a simplified network of hydrogen molecule formation and dissociation, beginning with the formation of the catalyst $H^-$. The formation rate coefficient of $H^-$ via radiative attachment, $H^\circ + e^- \rightarrow H^- + \gamma$, is $k_1 = (1.83 \times 10^{-18}) T^{0.8779}$ cm$^3$ s$^{-1}$ (Hutchings 1976). Destruction of $H^-$ is assumed to occur via three processes: (1) associative detachment ($H^- + H^\circ \rightarrow H_2 + e^-$) with a rate coefficient $k_2 = 1.35 \times 10^{-9}$ cm$^3$ s$^{-1}$ (Hutchings 1976); (2) photodetachment ($H^- + \gamma \rightarrow H^\circ + e^-$) with a rate $k_3 J_0 = (3.1 \times 10^{10}) J_0$ s$^{-1}$, using cross sections of Wishart (1979) and Broad & Reinhardt (1976) integrated over the MF spectrum above 0.755 eV threshold; and (3) mutual neutralization ($H^- + H^+ \rightarrow H^\circ + H^\circ$) with a rate coefficient $k_4 = (7 \times 10^{-7}) T^{-1/2}$ cm$^3$ s$^{-1}$ (Peart, Bennett, & Dolder 1985; Dalgarno & Lepp 1987). Since the $H^-$ formation rate is fast, $H^-$ will be in equilibrium, with a density,

$$n(H^-) = \frac{k_1 n_e n(H^\circ)}{[k_2 n(H^\circ) + k_3 J_0 + k_4 n(H^+)]} \,. \qquad (3)$$

In the limit when the rates $k_3 J_0$ and $k_4 n(H^+)$ are much smaller than $k_2 n(H^\circ)$, the $H^-$ density tracks the electron density, $n(H^-) = (k_1/k_2) n_e$.

We assume that the dominant formation process of $H_2$ is associative detachment, $H^- + H^\circ \rightarrow H_2 + e^-$, with rate coefficient $k_2$ (see above). The four dominant destruction processes for $H_2$ are taken to be (1) collisions with protons, $H_2 + H^+ \rightarrow H_2^+ + H^\circ$, with a rate coefficient $k_{D,H^+} = (6.4$

$\times 10^{-10}$ cm$^3$ s$^{-1}$) exp ($-2.65$ eV/$kT$) derived from detailed balance with the inverse reaction, using rates from Karpas, Anacich, & Huntress (1979); (2) dissociating collisions with electrons with rate coefficient $k_{D,e} = (5.6 \times 10^{-11}$ cm$^3$ s$^{-1})T^{0.5}$ exp ($-8.8$ eV/$kT$) derived from cross sections of Corrigan (1965); (3) dissociating collisions with H° using the low-density rate coefficient $k_{D,\mathrm{H}^\circ} = (6.11 \times 10^{-14}$ cm$^3$ s$^{-1}$) exp ($-4.48$ eV/$kT$) from Lepp & Shull (1983) and Mac Low & Shull (1986); and (4) UV photodissociation in Lyman and Werner bands with rate $k_{D,\gamma}J_0 = (1.23 \times 10^8)J_0$ s$^{-1}$ ($J_0$ in cgs units) computed from tabulated line oscillator strengths (Allison & Dalgarno 1970b), radiative dissociation fractions (Stephens & Dalgarno 1972), and line wavelengths (Namioka 1964; Morton & Dinerstein 1976) assuming a $\nu^{-1}$ energy spectrum across the 845–1108 Å band. We computed the direct continuum photodissociation rate ($\lambda \leq 844.87$ Å) to be over a factor of 60 smaller, $(1.87 \times 10^6)J_0$ s$^{-1}$ for an optically thin cloud, using cross sections of Allison & Dalgarno (1970a). Thus the molecular fraction can be derived from a single equation:

$$\frac{n(\mathrm{H}_2)}{n(\mathrm{H}^\circ)} = \left[\frac{k_2}{n(\mathrm{H}^\circ)k_{D,\mathrm{H}^\circ} + n(\mathrm{H}^+)k_{D,\mathrm{H}^+} + n_e k_{D,e} + k_{D,\gamma}J_0}\right] \times \left[\frac{k_1 n_e n(\mathrm{H}^\circ)}{k_2 n(H^\circ) + k_3 J_0 + k_4 n(\mathrm{H}^+)}\right]. \quad (4)$$

The molecular cooling rates were derived from fits to vibrational and rotational rates in Lepp & Shull (1983). We neglect $H_2 - H_2$ collisions.

### 2.4. *Calculational Technique*

Our model THERMAL first calculates the ionization state of the gas for a given temperature and an educated guess for the total hydrogen density. The heating and cooling is then calculated. If heating does not equal cooling, then the density of the gas is altered accordingly and the ionization state is recalculated. The process iterates until the heating equals cooling within 0.5%. We calculate thermal equilibrium ion populations for a range of temperatures, from 1500 K to the Compton temperature, which is dependent on the assumed incident spectral shape and is $2.5 \times 10^7$ K for the MF spectrum. We note that for sufficiently steep ionization spectra it is not possible to achieve a two-phase medium for the gas, an effect first pointed out by Guilbert, Fabian, & McCray (1983). If the EUV background is due simply to QSOs with steep spectra, something else must heat the intercloud medium (see also Miralda-Escudé & Ostriker 1990).

We calculate the equilibrium ionization parameter for two input spectra: (1) the MF spectrum; and (2) $f_\nu \propto \nu^{-1.5}$ for photon energies greater than 2.8 eV and $f_\nu \propto \nu^{-1}$ for photon energies less than 2.8 eV. For the MF spectrum we tested a range of metallicities $Z_\odot$ ranging from 0.01 to 0.3 times solar abundances. Here, $Z_\odot$ is the abundance relative to solar values (e.g., [C/H]) based on solar abundances from Grevesse (1984): 0.1, $4.9 \times 10^{-4}$, $9.8 \times 10^{-5}$, $8.1 \times 10^{-4}$, $3.5 \times 10^{-5}$, and $4.7 \times 10^{-5}$ for He, C, N, O, Si, and Fe, respectively. Below 0.01 solar metallicity, the thermal effects of heavy element radiative cooling are small, and the models converge to the same curves. For the $\nu^{-1.5}$ spectral shape, we test metallicities $Z_\odot = 0.01$ and 0.1. Our "standard" model assumes $Z_\odot = 0.1$ and a MF spectral shape.

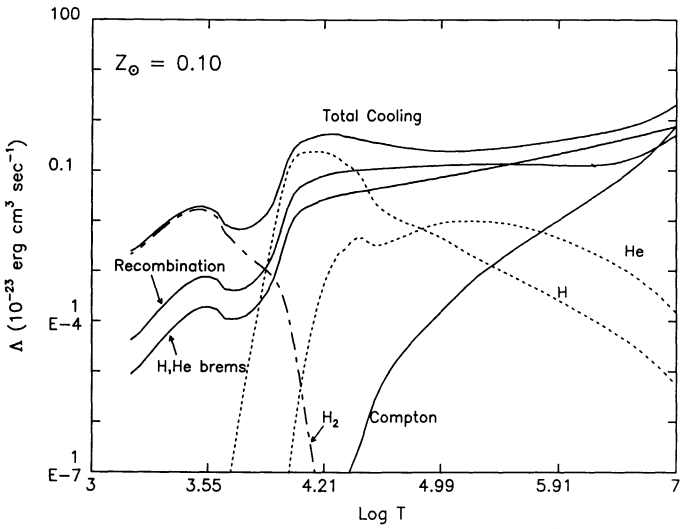


FIG. 1.—Cooling sources due to hydrogen and helium for a gas with 10% solar abundances irradiated by a MF (see text) spectral shape. Emissivity $\Lambda(T)$ (eV cm$^3$ s$^{-1}$) = $l/n_{\mathrm{H}}^2$ is shown as a function of temperature $T$.

## 3. RESULTS

### 3.1. *Temperatures and Neutral Fractions*

In Figures 1 and 2 we plot the contributions of the major coolants in our standard model. In these figures, the cooling function $\Lambda n_{\mathrm{H}}^2 \equiv l$, where $l$ (eV cm$^{-3}$ s$^{-1}$) is the total emissivity of the gas and $n_{\mathrm{H}}$ is the total hydrogen number density. The dominant coolants for temperatures from 8000–40,000 K are collisional excitation of H I, C I–IV, O I–VI, hydrogen and helium free-free emission (bremsstrahlung), and recombination cooling. Iron becomes a major coolant at $T \geq 10^6$ K. At 8000 K, the molecular fraction, $n(\mathrm{H}_2)/n(\mathrm{H\ I})$, increases to $\sim 4 \times 10^{-4}$, and at 5000 K increases to $\sim 2 \times 10^{-3}$. Thus at $T \lesssim 8000$ K, molecular cooling becomes important via vibrational excitation through collisions with neutral hydrogen. In Figure 3 we plot the contributions of the photoionization heat sources in our model. We neglect the effects of thermal conduction.

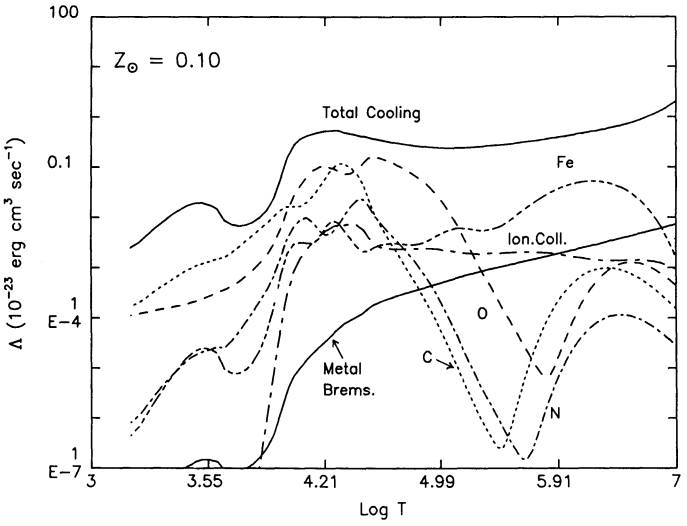


FIG. 2.—Metal cooling for model of Fig. 1

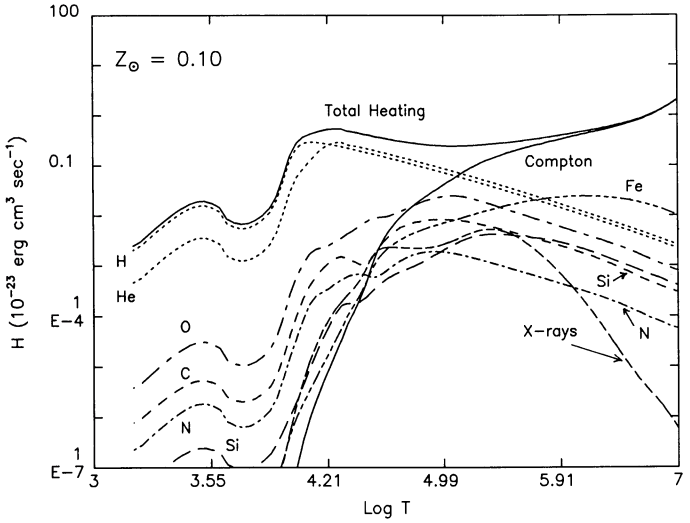


FIG. 3.—Heating sources for model of Fig. 1. Note that hydrogen and helium photoionization dominate for temperatures below 40,000 K, while Fe photoionization and Compton heating dominate above that temperature.

In Figure 4 we plot the equilibrium temperature against ionization parameter, $U = n_\gamma/n_H$. The addition of metals produces a lower equilibrium temperature for a given $U$, owing to the additional cooling by collisionally excited forbidden and fine structure lines. Metallicities $Z_\odot = 0.01$ and $Z_\odot = 0.0$ give identical results for $T > 10^4$ K, so for metallicities below 1% solar, the equilibrium temperatures are essentially the same. For $\log U \geq -3$, the $\nu^{-1.5}$ spectral shape gives a slightly higher equilibrium temperature than the MF spectral shape with the same metallicity. This occurs because of the higher neutral fraction and because photoelectric heating is most sensitive to the shape of the input spectrum in the EUV energy band (the MF spectral shape steepens from $\nu^{-1.0}$ to $\nu^{-3}$ in the energy range 24–365 eV). Most importantly, in order to reduce the equilibrium temperatures below $10^4$ K, $\log U$ must be less than $-4.3$ to $-5.0$ (see Table 1). Molecular cooling enables the gas to cool to temperatures below $10^4$ K without exceeding total hydrogen densities of $\sim 1$ cm$^{-3}$ if $J_0 \approx 10^{-21}$ ergs s$^{-1}$ cm$^{-2}$ Hz$^{-1}$.

We can fit the cloud temperature $T$ to a power law in $U$ over the relevant range for the standard model (MF spectrum, $Z_\odot = 0.1$):

$$T = (3.6 \times 10^4 \text{ K}) U^{0.118}, \quad (-4.7 < \log U < -1.8). \quad (5)$$

We can also fit a power law to the same variables for $Z_\odot = 0.01$ and the MF spectral shape:

$$T = (4.9 \times 10^4 \text{ K}) U^{0.152}, \quad (-4.3 < \log U < -1.7). \quad (6)$$

The corresponding Doppler parameters, $b = (2kT/m_H)^{1/2}$, for H I absorption lines in these temperature fits are, for a MF spectrum and $Z_\odot = 0.1$:

$$b = (24 \text{ km s}^{-1}) U^{0.059}, \quad (-4.7 < \log U < -1.8). \quad (7)$$

For a MF spectrum and $Z_\odot = 0.01$:

$$b = (28 \text{ km s}^{-1}) U^{0.076}, \quad (-4.3 < \log U < -1.7). \quad (8)$$

In Figure 5 we plot the equilibrium neutral fraction as a function of $U$, where we again see the effects of the spectral shape in the EUV region. For the $\nu^{-1.5}$ spectrum, the neutral fraction is slightly higher for a given $U$ than for the MF spec-

TABLE 1

SOME EQUILIBRIUM VALUES OF log ($U$)

| PARAMETER | $T$(K) 8000 | 10,000 | 12,000 |
|---|---|---|---|
| MF: | | | |
| $Z_\odot = 0.3$ ..... | −5.3 | −4.3 | −3.2 |
| $Z_\odot = 0.1$ ..... | −6.2 | −4.7 | −3.5 |
| $Z_\odot = 0.01$ ..... | −7.1 | −5.0 | −3.8 |
| $\nu^{-1.5}$: | | | |
| $Z_\odot = 0.1$ ..... | −6.1 | −4.7 | −3.9 |
| $Z_\odot = 0.01$ ..... | −7.0 | −4.9 | −4.1 |

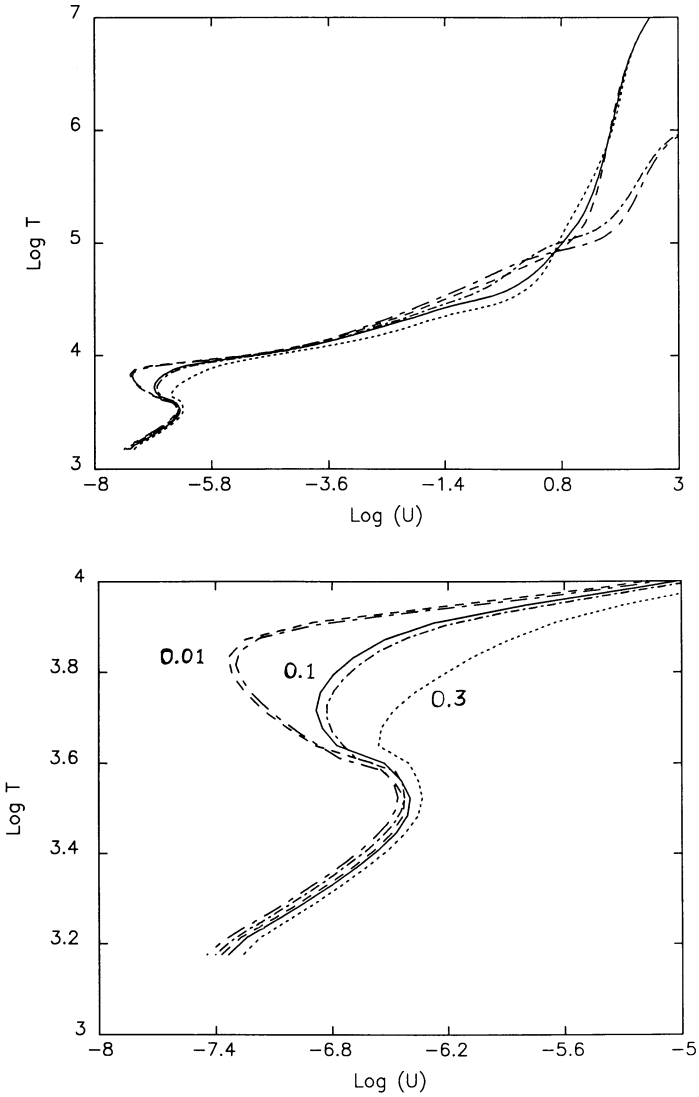


FIG. 4.—Temperature as a function of ionization parameter, $U$, the ratio of ionizing photons to total hydrogen density. The dotted line represents a MF spectrum with $Z_\odot = 0.3$. The solid line corresponds to a MF input spectrum with $Z_\odot = 0.1$, and the dashed line corresponds to MF input spectrum with $Z_\odot = 0.01$. The dash-dot line corresponds to a $\nu^{-1.5}$ spectrum with $Z_\odot = 0.1$, and the dash-short dash line is the same spectrum with $Z_\odot = 0.01$. Gas with $Z_\odot = 0.01$ has the same thermal characteristics as zero metallicity gas.

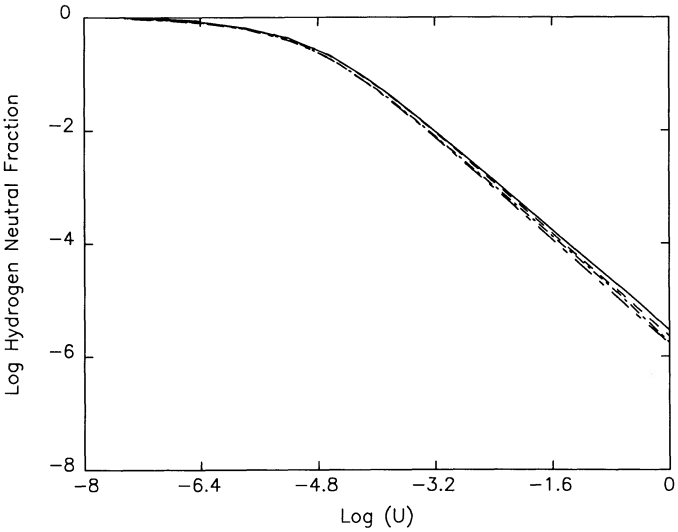


FIG. 5.—The hydrogen neutral fraction as a function of ionization parameter, $U$. The lines correspond to the same models as described in Fig. 4.

tral shape. The difference between the neutral fractions obtained for the various models is not more than a factor of 2 for a given $U$ in any case. We can fit a power law to the neutral fraction for relevant ionization parameters in the standard model,

$$\frac{n(\mathrm{H\ I})}{n_{\mathrm{H}}} = (4.6 \times 10^{-6})U^{-1.026}, \quad -4.7 < \log U < -1.8 . \tag{9}$$

For a MF spectrum and $Z_{\odot} = 0.01$:

$$\frac{n(\mathrm{H\ I})}{n_{\mathrm{H}}} = (3.4 \times 10^{-6})U^{-1.066}, \quad -4.7 < \log U < -1.8 . \tag{10}$$

Figure 6 shows the fractional ionization of all ion stages of C, N, O, Si, and Fe as a function of $U$. In Figure 7 we plot the column densities of the ions with observable absorption lines, Si II, Si III, Si IV, C II, C III, C IV, N V, and O VI, divided by the column density of H I, as a function of log $U$. In our models, C IV has a higher column density than C II for log $U \gtrsim -2.9$ (MF spectrum). This is comparable to similar models for a cloud with $N(\mathrm{H\ I}) = 10^{17.4}$ cm$^{-2}$ by Steidel & Sargent (1989) in which C IV is greater than C II for log $U \gtrsim -2.6$.

Since the rate coefficients for charge exchange with neutral hydrogen are slow for "recombination" to C I and C II, these ions are not greatly affected by charge exchange. However, for charge exchange to C III and C IV, the rates are very high; thus, as the H° neutral fraction increases above $10^{-2}$ charge exchange becomes dominant. Additionally, charge transfer rates between Si II and Si III are not only fast, but fast in both directions (Baliunas & Butler 1980) because of a near-resonant crossing to the Si II ground state. Thus the Si II/Si III ratio is driven by the H I/H II ratio when the neutral fraction exceeds $\sim 10^{-2}$. Because of these effects, the column density of Si IV remains comparable to that of Si III for log $U \lesssim -2.3$, in contrast with the Steidel & Sargent (1989) result of log $U \lesssim -1.4$. In this instance our code predicts a somewhat higher ionization state for a given ionization parameter than does CLOUDY (Ferland 1989), a versatile photoionization code which incorporates radiation transfer and high-density effects. The difference in results appears to be due to slight differences in charge-exchange rate coefficients of Si ions with H I, since the Opacity Project photoionization cross sections for Si III and Si IV are within 10%, at threshold, of those used in CLOUDY.

### 3.2. *Thermal Phases*

For each model, we plot a phase curve of log $(U/T)$ versus $T$ in Figure 8. These diagrams can be used to illustrate the presence of two or more stable phases for a single ratio of radiation-to-gas pressure, proportional to $U/T$ (Lepp et al. 1985). A steep spectral shape such as $f_{\nu} \propto \nu^{-1.5}$ precludes the existence of a two-phase medium (Guilbert et al. 1983). Another important point is that for values log $(U/T) < -6$, characteristic of the intergalactic medium (IGM), two stable phases cannot coexist. If the clouds are confined by the pressure of a warmer, more tenuous medium, this medium cannot be heated by metagalactic UV flux of the spectral shapes we discuss here.

If the cloud-intercloud medium does coexist in pressure equilibrium, as would be obtained with a MF spectral shape and a rather large ionization parameter, we can derive the maximum thermal velocity of H I absorption lines created in QSO spectra by these clouds. If the maximum thermal velocity is small enough, we would be able to rule out a thermal source for line widths greater than this velocity and could hypothesize that the line widths may be created by line blending. However, for metallicities $Z_{\odot} = 0.01$–$0.3$ times solar abundances, the maximum $b$-value we obtain for H I is 52–56 km s$^{-1}$, a value which is not restrictive of the interpretation of current observations. These $b$-values correspond to temperatures of $T =$ 160,000–190,000 K, and log $U \sim 0.9$–$1.2$. The maximum ionization parameter is substantially higher than that derived from observations of metal ion abundances in intergalactic clouds. Thus, the fact that the line widths imply cloud temperatures at or below 30,000 K means that the Ly$\alpha$ clouds do not exist in two-phase equilibrium, heated and ionized by quasars. Pressure confinement of these clouds therefore remains a problem.

We can further derive from these phase curves that between equilibrium temperatures $T_{\mathrm{eq}}$ of 2800 K and either 4800 K ($Z_{\odot} = 0.3$) or 6000 K ($Z_{\odot} \leq 0.01$) the gas is thermally unstable, since $dT_{\mathrm{eq}}/dU < 0$. For $J_0 = 10^{-21}$ ergs s$^{-1}$ cm$^{-2}$ Hz$^{-1}$, the cooling time for the gas at these densities and temperatures is $\sim$2000–4000 yr. The stable temperature ranges correspond to H I Doppler parameters $b \leq 6.8$ km s$^{-1}$ and $b \geq 9$–$10$ km s$^{-1}$ for $Z_{\odot} = 0.3$.

For temperatures below $10^4$ K and $I_0 = 10^{-21}/4\pi$ ergs s$^{-1}$ cm$^{-2}$ Hz$^{-1}$ sr$^{-1}$, we find that the equilibrium densities for optically thin clouds are required to be $\gtrsim 1$ cm$^{-3}$ in order to provide sufficient cooling to counteract the photoelectric heating of the clouds. If the clouds are truly at temperatures $T < 10^4$ K, even with molecular cooling, the hydrogen density of the clouds still must be high ($n_{\mathrm{H}} \gg 10^{-3}$ cm$^{-3}$). Therefore, based on the observed H I column densities, the cloud thicknesses must be much smaller than previously supposed. A limit to the molecular fraction in the gas is imposed due to the lack of observed $H_2$ Lyman absorption bands associated with the stronger H I absorption lines. This is not a strong constraint, however, since only a trace molecular component in the gas will contribute strongly to the cooling, whereas column densities $N(H_2) \geq 2 \times 10^{14}$ cm$^{-2}$ are required to provide detect-

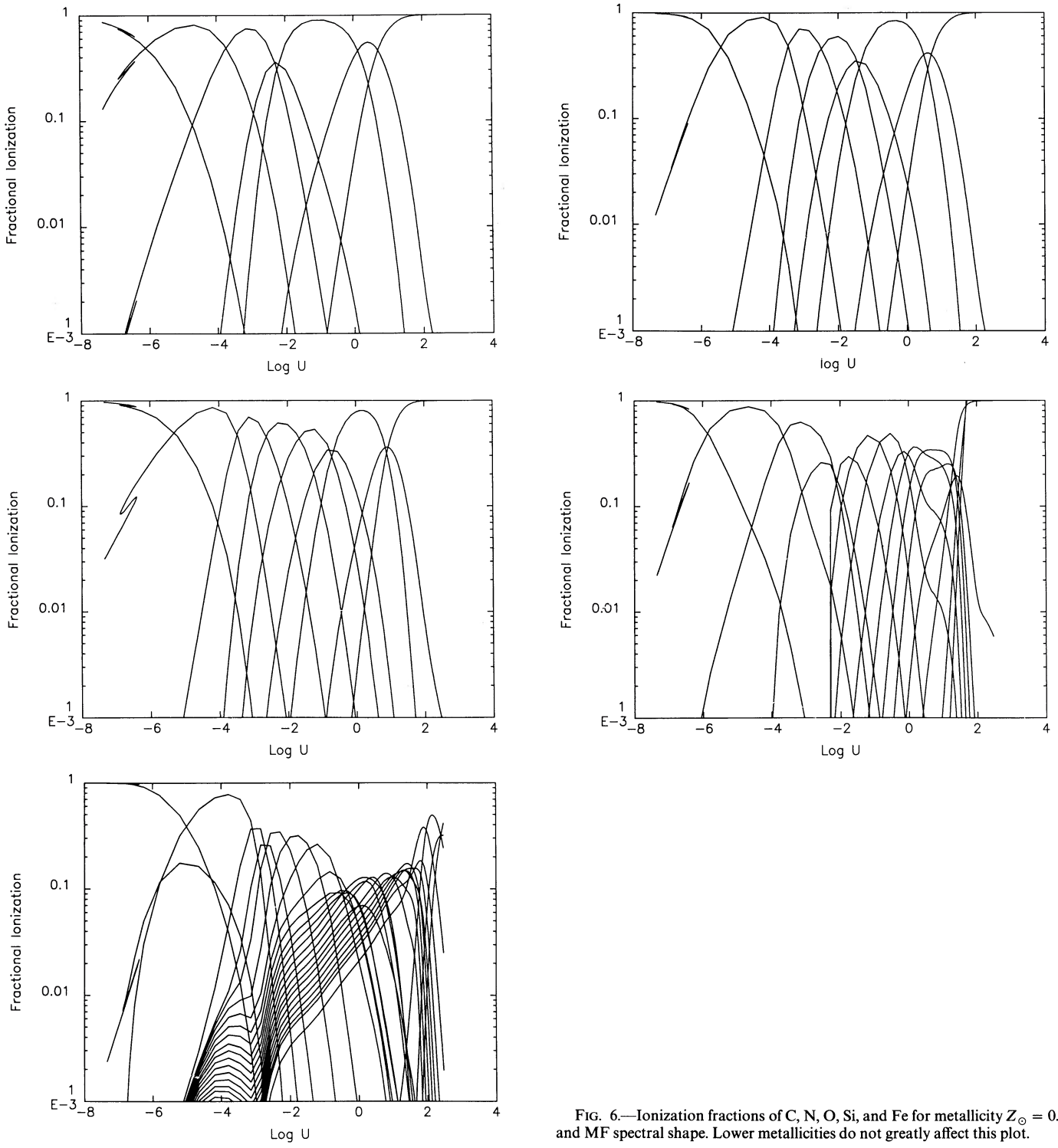


FIG. 6.—Ionization fractions of C, N, O, Si, and Fe for metallicity $Z_{\odot} = 0.1$ and MF spectral shape. Lower metallicities do not greatly affect this plot.

able (20–30 mÅ) $H_2$ rest frame equivalent widths in the Lyman (3–0) $R(1)$ (1063.460 Å) and (4–0) $R(1)$ (1049.958 Å) lines when $T \approx 2000$ K. The molecular fraction of the gas versus $U$ is shown in Figure 9, and the fraction versus $T$ is shown in Figure 10.

### 3.3. *Analytic Approximations*

We have found that the inclusion of metals does not affect the thermal balance of the cloud until the metallicity is at least 1% solar. For lower metallicities the thermal behavior can be modeled by a gas with primordial abundances. Most of the "Ly$\alpha$ forest" clouds are optically thin to EUV radiation; optical depth unity in the Lyman continuum is reached at a column density $N(\mathrm{H\ I}) = (10^{17.2}\ \mathrm{cm}^{-2})(E/13.6\ \mathrm{eV})^3$. Thus, an enhanced ionization parameter $U$ (or $J_0/n_{\mathrm{H}}$) will decrease the neutral fraction, $f_0 = n(\mathrm{H}^{\circ})/n_{\mathrm{H}}$, and slightly raise the temperature $T$.

We may estimate these effects with a simple model (see also

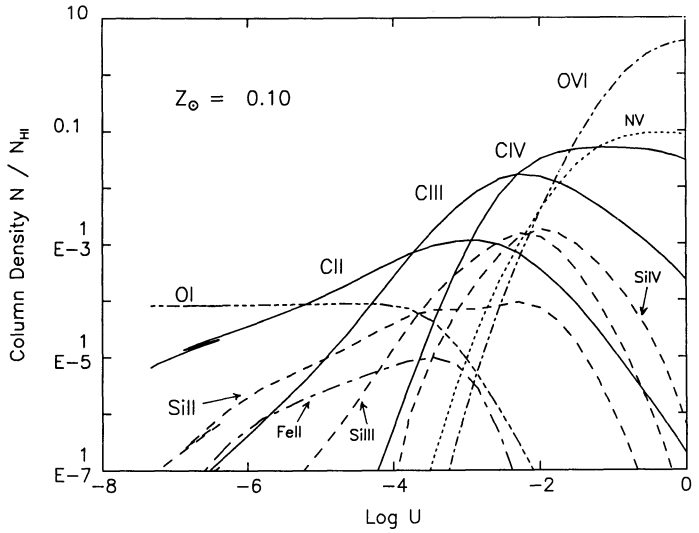


FIG. 7.—Observable absorption lines. Ratios of column densities of observable ion species to neutral hydrogen. The standard model was assumed here (MF spectrum, $Z_\odot = 0.1$).

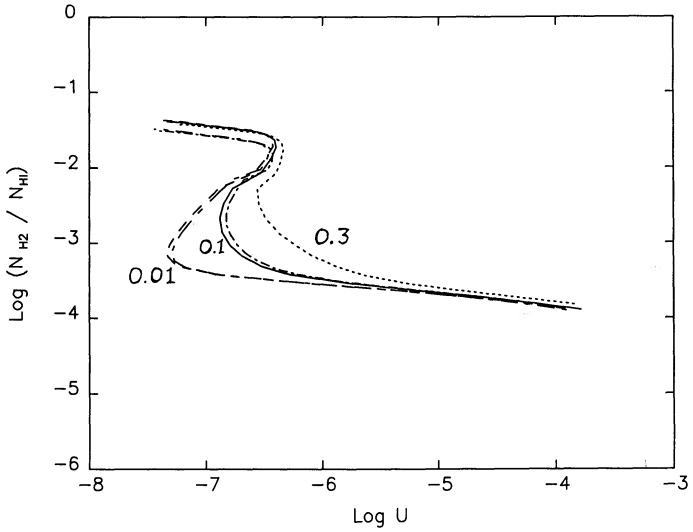


FIG. 9.—Ratio of $H_2$ density to total hydrogen number density as a function of ionization parameter $U$. Note the effect of metallicity on the minimum $U$ obtained.

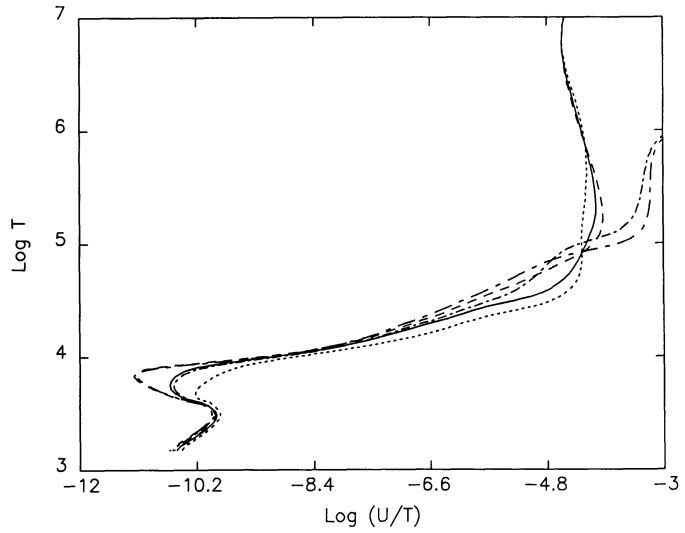


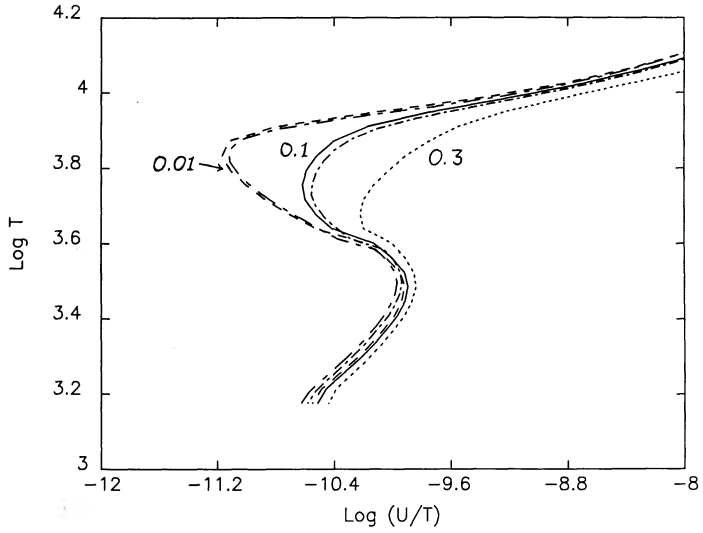


FIG. 8.—Thermal phase plot, with the same line code as Fig. 4

Black 1981) of a highly ionized intergalactic cloud of hydrogen density $n_H = (10^{-3}\ \mathrm{cm}^{-3})n_{-3}$ exposed to an ionizing flux $J_0 = (10^{-20}\ \mathrm{ergs\ cm^{-2}\ s^{-1}\ Hz^{-1}})J_{-20}$. If we approximate the hydrogen photoionization cross section by $\sigma(\nu) = \sigma_0(\nu/\nu_0)^{-3}$, with $\sigma_0 \approx 6.3 \times 10^{-18}\ \mathrm{cm}^2$ and $h\nu_0 = 13.6$ eV, the photoionization rate $\Gamma_i(\mathrm{s}^{-1}) = (\sigma_0 J_0/4h)$ and the photoelectric heating rate $H_i\ (\mathrm{ergs\ s}^{-1}) = (\sigma_0 J_0 \nu_0/12)$, for an ionizing spectrum $f_\nu \propto \nu^{-1}$. The mean energy of the photoelectrons is $h\nu_0/3$ in this model. The recombination plus free-free cooling rate coefficient may be written $\alpha_H^{(2)}\beta kT$, where $\alpha_H^{(2)}(T) \approx (2.59 \times 10^{-13})T_4^{-0.845}\ \mathrm{cm}^3\ \mathrm{s}^{-1}$ is the rate coefficient for hydrogen recombination to excited states and $\beta \approx 1.13$ for the temperatures of interest ($T_4$ is the temperature in units of $10^4$ K). If photoionization and collisional ionization balance radiative recombination, and if photoelectric heating balances cooling by recombination, bremsstrahlung, and electron-impact exci-

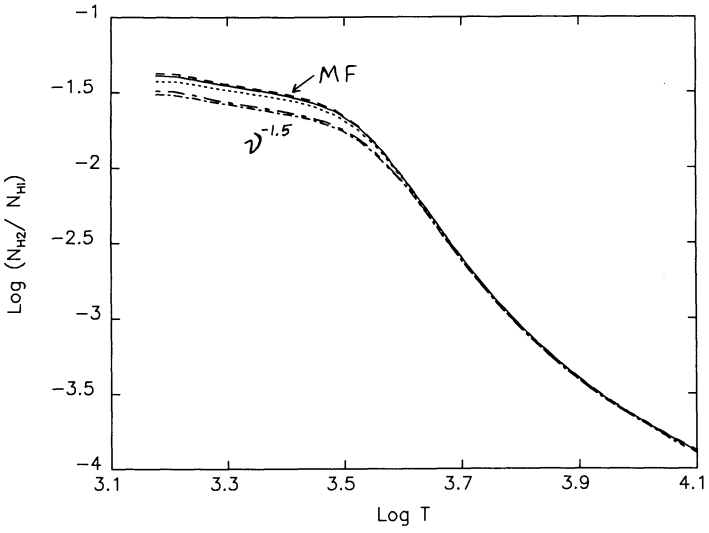


FIG. 10.—Ratio of $H_2$ to H I column density vs. temperature $T$

tation and ionization of H I, we find

$$\frac{n(\mathrm{H}^0)}{n_\mathrm{H}} = \left(\frac{4h\alpha_\mathrm{H}^{(2)} n_\mathrm{H}}{\sigma_0 J_0}\right)[1 + (a_2 n_\mathrm{H}/J_0)]^{-1} \quad (11)$$

$$T = \left(\frac{h\nu_0}{3\beta k}\right)\left[\frac{1 - (a_1 n_\mathrm{H}/J_0)}{1 + (a_2 n_\mathrm{H}/J_0)}\right], \quad (12)$$

with $a_1 = (12h/\sigma_0)[0.75C_e(T) + C_i(T)]$ and $a_2 = (4h/\sigma_0)C_i(T)$, where $C_i(T)$ and $C_e(T)$ are rate coefficients (cm$^3$ s$^{-1}$) for electron-impact ionization and ($n = 2$) excitation of H I. Thus, the characteristic values of temperature and neutral fraction are $T \leq (h\nu_0/3\beta k) \approx 47{,}000$ K and $f_0 = (4h\alpha_\mathrm{H}^{(2)} n_\mathrm{H}/\sigma_0 J_0) \approx (10^{-4}) n_{-3} J_{-20}^{-1} T_4^{-0.845}$. To obtain greater accuracy, equations (11) and (12) may be solved iteratively for $T$ and $f_0$ in terms of the "ionization parameter," $J_0/n_\mathrm{H}$. For pure hydrogen, $T$ and $f_0$ range between (27,000 K; $4.6 \times 10^{-5}$) and (39,000 K; $3.4 \times 10^{-6}$) for $(J_0/n_\mathrm{H}) = 10^{-17}$ to $10^{-16}$ ergs cm s$^{-1}$ Hz$^{-1}$. The inclusion of helium increases the temperature somewhat due to photoelectric heating of He$^+$.

## 4. CONSEQUENCES OF THE MODELS

### 4.1. *Cold Lyman-α Clouds?*

Recent observations at 6.5 km s$^{-1}$ resolution of Lyα forest clouds with $12.7 \leq \log N(\mathrm{H\ I}) \leq 14.0$ toward QSO 2206−199N (Pettini et al. 1990) suggest that many Lyα lines have Doppler parameters $b \leq 22$ km s$^{-1}$. If the $b$-value is thermal, this implies that $T < 30{,}000$ K, the value generally assumed for Lyα clouds. Pettini et al. further suggest that most of this line broadening is caused by large-scale motions, since they find that $b$ and $N$(H I) are correlated; a relation $N(\mathrm{H\ I}) = (8.7 \times 10^{12}\ \mathrm{cm}^{-2})(b/10\ \mathrm{km\ s}^{-1})^{2.1}$ may be fitted to their data, which implies that the Lyα lines have line-center optical depths $\tau_0 = (1.2)(b/10\ \mathrm{km\ s}^{-1})^{1.1}$, indicating that most of the lines are only weakly saturated. If the line broadening is dominated by large-scale motions, an estimate of the temperature can be derived from the minimum resolved line widths, $b \sim 10$ km s$^{-1}$ or $T \sim 6000$ K.

Our models suggest that, for a background ionizing spectrum normalized at 13.6 eV to $J_\nu = 10^{-21}$ ergs s$^{-1}$ cm$^{-2}$ Hz$^{-1}$, the total hydrogen densities in a cloud at $T = 10^4$ K must be 0.2–0.5 cm$^{-3}$. Variations in these estimates are due to different input spectral shapes and a range of metallicities $Z_\odot = 0$–0.1. These clouds are mostly neutral, with $n(\mathrm{H\ I})/n_\mathrm{H} \sim 0.3$. Thus, the characteristic cloud thickness along the line of sight of such a cloud is (1.8–36) $\times 10^{-5}$ pc. A similar result was obtained by Pettini et al. (1990) using CLOUDY. This thickness is in contrast to the transverse size of clouds of $d \sim 10h^{-1}$ kpc, where $h = (H_0/100\ \mathrm{km\ s}^{-1}\ \mathrm{Mpc}^{-1})$, estimated by Foltz et al. (1984), or the revision of this estimate, $d \sim 100h^{-1}$ kpc, by Steidel & Sargent (1990), and with the requirement that Lyα clouds fully cover the QSO emission-line region ($d > 1$ pc) (Sargent et al. 1980). Thus, it appears that these clouds are sheetlike, with aspect ratios of $10^5$–$10^9$. Such geometries are difficult to understand, but they could perhaps be formed and confined by shock ram pressure. Maintaining a narrow line width across the cloud would be difficult.

We may derive a direct estimate of $J_0 = J_\nu(13.6\ \mathrm{eV})$ in QSO 2206−199N from an analysis of the QSO's observed B magnitude and the redshift difference between the emission and absorption lines. Emission redshifts have been published (Sargent, Boksenberg, & Steidel 1988) for C IV ($z_e = 2.553$), Si IV + O IV] ($z_e = 2.556$) and Lyα ($z_e = 2.575$), for a weighted mean of $z_e = 2.559$. Because the Lyα emission redshift is smaller than those of absorption system 100 ($z_a = 2.58487$) and system 101 ($z_a = 2.58658$), the "true" (ionization source) emission redshift, as defined by Hα and the low-ionization lines, is probably shifted beyond $z_e = 2.59$. As is well known from studies of quasar spectra (Gaskell 1982; Wilkes & Carswell 1982; Espey et al. 1989; Corbin 1990), the high-ionization emission lines (e.g., C IV λ1549, C III] λ1909) are systematically blueshifted relative to the low-ionization lines (e.g., Mg II λ2800, Balmer lines). In his survey of emission-line redshift differences, Corbin (1990) found that the redshift difference between Mg II and C IV occasionally exceeded 4000 km s$^{-1}$ in a sample of high-redshift, high-luminosity, optically selected QSOs; the mean value of the difference was ∼1700 km s$^{-1}$ and the extreme value was 4800 km s$^{-1}$. In order for QSO 2206−199N to lie behind system 101, the redshift difference must be at least 2830 km s$^{-1}$.

Lacking a reliable (Hα) redshift for the true rest frame of the ionizing source in QSO 2206−199N, we adopt $z_e = 2.605$, since $z_e = 2.600$ corresponds to a C IV − Hα redshift difference of 4000 km s$^{-1}$ and $z_e = 2.610$ corresponds to 4800 km s$^{-1}$. The proper distance to the QSO and the absorption systems is given by the formula (Weinberg 1972)

$$d(z) = \left(\frac{c}{\mathrm{H}_0}\right)\left\{\frac{q_0 z + (q_0 - 1)[(1 + 2q_0 z)^{1/2} - 1]}{q_0^2(1 + z)}\right\}. \quad (13)$$

The difference in proper distance between the QSO and the absorption clouds is therefore (8.8–21.9 Mpc)$h^{-1}$ (system 100) and (8.1 − 20.0 Mpc)$h^{-1}$ (system 101), for $q_0$ in the range 0.1–0.5 (larger distances for smaller $q_0$.) The quasar's magnitude $B = 17.49$ translates to an *observed* monochromatic flux $f_\nu(4400\ \text{Å}) = 4.4 \times 10^{-27}$ ergs cm$^{-2}$ s$^{-1}$ Hz$^{-1}$ (Weedman 1986), *emitted* at $\lambda_e = 1220$ Å. Using the relation $L_{\nu,e} = 4\pi d^2 (1 + z) f_{\nu,0}$ and extrapolating to 912 Å with a QSO power law of $f_\nu \propto \nu^{-0.5}$ (MF), we find that the QSO has an *emitted* spectral luminosity $L_{\nu,e} = (1.3\text{–}2.9 \times 10^{31}$ ergs s$^{-1}$ Hz$^{-1})h^{-2}$ at 912 Å, for a range $q_0 = 0.1$–0.5 (larger luminosity at smaller $q_0$).

We therefore derive a minimum ionizing flux of $J_\nu = (0.5\text{–}1.4) \times 10^{-21}$ ergs s$^{-1}$ cm$^{-2}$ Hz$^{-1}$ at the position of absorption system 100, and $J_\nu = (0.6\text{–}1.7) \times 10^{-21}$ ergs s$^{-1}$ cm$^{-2}$ Hz$^{-1}$ at system 101, where the range of values corresponds to $q_0 = 0.1$ to 0.5 (higher flux for larger $q_0$). This flux is about 10 times smaller than the Lyman-limit metagalactic flux for $1.8 \leq z \leq 3.8$, $J_\nu = 4\pi \times 10^{-21}$ ergs s$^{-1}$ cm$^{-2}$ Hz$^{-1}$, estimated from the "proximity effect" (Bajtlik et al. 1988). An ionization parameter $\log U \approx -6$ is needed to explain the observed Doppler parameters in absorption system 100 ($b = 7.5$ km s$^{-1}$) and 101 ($b = 10$ km s$^{-1}$). Therefore, $n_\mathrm{H} \approx 5$ cm$^{-3}$ is required if $J_0 \approx 10^{-21}$ (cgs) for a "MF" ionizing spectrum. The cloud thicknesses, $N(\mathrm{H\ I})/n_\mathrm{H}$, of systems 100 and 101 are then just $10^{12}$ cm.

The origin of the cloud thicknesses cannot easily be reconciled with cooling layers behind radiative shocks, with thermal instabilities, or with gravitational collapse. The scales associated with radiative shocks and thermal instabilities are of order a cooling length, about 1 pc for $T = 10^4$ K, metallicity $Z_\odot = 0.1$, and $n_\mathrm{H} \sim 0.3$ cm$^{-3}$, far too large to explain the tiny thicknesses of the clouds. Gravitational collapse via Jeans instability gives a thickness of order (680 pc) $(T_4/\mu n_\mathrm{H})^{0.5}$, where $\mu$ is the mean weight per particle divided by the hydrogen mass. A preliminary sketch of a scenario where Lyα clouds

form behind shocks in pregalactic halos was presented by Hogan (1987); but in order for the neutral hydrogen column densities to be $\sim 10^{12.7}$–$10^{14}$ cm$^{-2}$ and for the cloud temperature to be below $10^4$ K with $J_0 \sim 10^{-21}$ ergs cm$^{-1}$ s$^{-1}$ Hz$^{-1}$, the cloud thickness is much less than a shock thickness.

Further the inferred pressures in the low-$T$ clouds would be $P \sim 4 \times 10^{-13}$ ergs cm$^{-3}$. Suppose that these clouds are confined by the thermal pressure of a tenuous IGM with H density $n_{\rm IGM} = (8.02 \times 10^{-6}$ cm$^{-3})\Omega_I h^2(1+z)^3$, where $\Omega_I$ is the closure parameter of smoothly distributed IGM. The IGM temperature then needs to be $T_{\rm IGM} = (3.7 \times 10^8$ K$)\Omega_I^{-1}h^{-2}(1+z)^{-3}$. If these clouds are indeed at $T \leq 10^4$ K, they are not confined by a baryonic IGM. They might be confined gravitationally by massive dark matter halos (Rees 1986), but it would be difficult to explain the extremely large ratio of dark matter to baryon mass unless the H I existed only at the center of a more extended structure of warmer, ionized gas.

Adiabatic cooling by rapid cloud expansion would allow high-pressure Ly$\alpha$ clouds to remain cool, yet less dense than an equilibrium photoionization model would allow. However, the clouds would be heated within $\sim 10^4$ yr for $J_0 \sim 10^{-21}$ ergs cm$^{-2}$ s$^{-1}$ Hz$^{-1}$. A high-density ($n_{\rm H} \approx 1$ cm$^{-3}$) cloud of column density $(10^{13}$ cm$^{-2})N_{13}$ would expand on a time scale of (0.3 yr)$N_{13}n_{\rm H}^{-1}T_4^{-1/2}$, leaving one to wonder how they are replenished. It seems unlikely that this mechanism is important for high-pressure Ly$\alpha$ clouds. However, adiabatic cooling could be an important mechanism for lowering the temperatures of low-pressure clouds (Duncan, Vishniac, & Ostriker 1991). We explore these possibilities in a later paper (Shull & Donahue 1992).

Another possible mechanism to keep clouds cold would be to allow the photoelectrons to escape the cloud rather than heating it. If the cloud thickness is very thin, the photoelectrons may escape the cloud without energy losses. The electron column density required to stop a 10 eV photoelectron by Coulomb collisions is $\sim 10^{13}$ cm$^{-2}$. We mimicked this process by reducing the photoelectric heating of the gas by a factor $f = 0.5$, 0.2, and 0.1. In order for this mechanism to have an effect, the clouds must have a low electron density. We plot our results for our standard model with reduced photoelectric heating in Figure 11. The effect on the thermal balance of the cloud can be quite dramatic, even for $f \approx 0.5$, and would decrease with increasing cloud column density. This may explain some of the observed correlation of $b$-value with column density (Pettini et al. 1990).

An offsetting mechanism would be electron confinement by a magnetic field. The gyroradius of an electron of energy (10 eV)$E_{10}$ is $\sim(10^{13}$ cm$)E_{10}^{0.5}B_{-12}^{-1}$ for a magnetic field of $(10^{-12}$ G$)B_{-12}$. This effect is important for an organized field aligned along the long axis of the clouds and completely confined within the cloud, since an electron could easily escape along a $B$-field which threads the cloud. It is difficult to imagine how a $B$-field would be aligned along the long axis of the cloud, since collapse of a cloud would most naturally occur perpendicular to the orientation of the $B$-field. Additionally, this mechanism could be slowed if the clouds became sufficiently positively charged due to the loss of electrons. However, electric fields would not have a chance to develop due to the attraction of thermal, less energetic electrons from the IGM to the charged cloud. This mechanism would easily short out any fields unless the density contrast was greater than about six orders of magnitude.

However, photoelectron escape does not explain how to maintain the large aspect ratios implied by the sizes of the clouds derived from double-QSO experiments (Foltz et al. 1984; Steidel & Sargent 1990) and the large neutral fractions required to achieve the low temperatures in a static model.

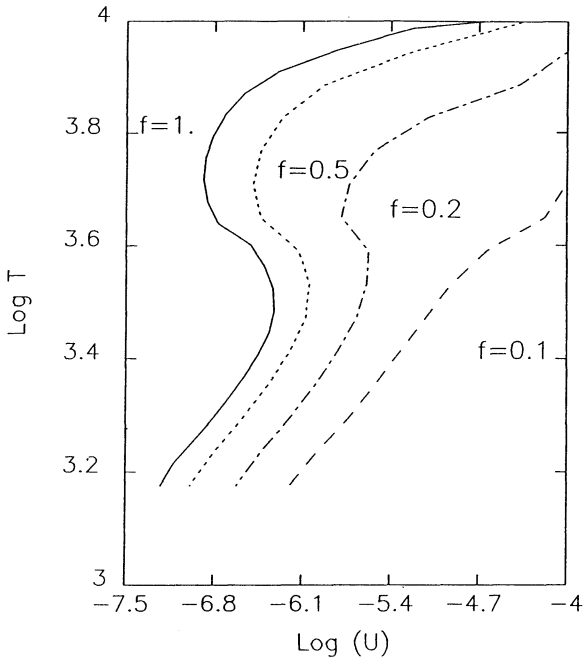


FIG. 11.—Auger and photoelectron escape. Modification to the low-temperature end of the equilibrium values of temperature and ionization parameter $U$ if a fraction $(1-f)$ of photoelectrons is allowed to escape a narrow slab of gas rather than heating it.

### 4.2. *Metallicities*

Limits on the equivalent widths of metal absorption lines have been obtained by Chaffee et al. (1985, 1986). If we assume that the $z = 3.321$ system in the quasar S5 0014+81 has a column density (cm$^{-2}$) of log $N$(H I) = 16.5 (an average of the 16.3 and 16.7 measured for the double system), we can derive the upper limit to the system's metallicity from the upper limits to the column densities of the ions C II, C III, and C IV. No real metallicity information is contained in C II, but the C III and C IV upper limits give interesting limits to the metallicity if the ionization parameter $U$ is sufficiently high. For example, if log $U = -2$, then the derived upper limit to the metallicity is $Z_\odot < 7 \times 10^{-4}$. However, if log $U = -5$, the metallicity is limited only to $Z_\odot < 0.1$.

A system which is marginally optically thick, $N$(H I) = $10^{17.35\pm0.1}$ cm$^{-2}$, was observed by Sargent, Steidel, & Boksenberg (1990) at $z = 2.9676$ in the quasar spectrum PKS 2126−158. If we assume that the reported column densities of C II and C IV are real detections, then, since we know the relative ion fractions of C II and C IV, we can specify log $U = -3.0 \pm 0.1$ and find that [C/H] = $-2.2 \pm 0.2$, where [C/H] is the logarithmic abundance of carbon relative to the solar abundance.

Spectra of Ly$\alpha$ systems in four QSOs were combined by Williger et al. (1989) in order to search for heavy element systems. Their limits on the composite system could potentially be used to constrain the metallicity of these clouds, if $U$ were known a priori. If log $U \leq -5$, as suggested by the Pettini et al. (1990) observations, no interesting metallicity limit can be

placed on these clouds, even if they are in dynamic and ionization equilbrium.

### 4.3. *Limits on Ionization Parameter for Metal-Line Systems*

An interesting observation is that C IV is almost always stronger than C II in sharp, optically thin metal-line systems (e.g., Wolfe 1983); C II is not necessarily present. If we know the shape of the ionizing background we can then derive the minimum ionization parameter required. For our spectral model MF, we find $N(\text{C IV}) > N(\text{C II})$ for $\log U > -2.9$, corresponding to temperatures $T \gtrsim 1.5 \times 10^4$ K. The observed value of $N(\text{Si III})/N(\text{Si IV})$ is of order 1 – 3 (Bergeron & Stasinka 1986). This restricts $\log U$ to be less than $-2.1$ (Blades et al. 1985).

The resulting limit on $U$ for the narrow-line metal systems is $-3.1 \leq \log U \leq -2.1$. The corresponding metallicity limits are $\log (Z_\odot) \leq -2.2$. Similar exercises can be done for other spectral shapes. However, for plausible QSO spectral shapes, the results do not change much.

## 5. CONCLUSIONS

If Ly$\alpha$ forest clouds are indeed much cooler than the previously assumed value, $T = 30{,}000$ K, the ionization parameter must be very low, even with the cooling contribution of a trace component of molecules. If the clouds cool below $T \sim 6000$ K, their final equilibrium must be $T < 3000$ K, owing to the lack of a stable phase between 6000 and 3000 K. At such low temperatures and high densities, one cannot constrain the metal content of these clouds. Even a solar abundance of metals could easily be hidden in cool clouds. If we assume that the clouds are being irradiated by a EUV power-law continuum typical of QSOs, with $J_0 = 10^{-21}$ ergs s$^{-1}$ cm$^{-2}$ Hz$^{-1}$, we derive typical cloud thicknesses along the line of sight that are much smaller than would be expected from shocks, thermal instabilities, or gravitational collapse. Further, the cloud pressure approaches that of the interstellar medium, $P/k \approx 10^{3-4}$ cm$^{-3}$ K, and the clouds cannot be confined by the pressure of the IGM.

Photoelectron escape from thin, neutral clouds would keep the clouds at colder temperatures than they would have if the photoelectrons were able to deposit all of their energy as heat via Coulomb collisions. This mechanism, although a promising mechanism for keeping the clouds colder than simple photoionization equilibrium models would predict, still does not explain how these clouds might be so thin. In order for adiabatic expansion to keep clouds cold as they expand, the heating time in the clouds must be long compared to the ionization and expansion time. Additionally, the heating time would need to be either longer than the Hubble time or tuned to a formation rate in order to explain the presence of numerous Ly$\alpha$ clouds over redshifts from $z = 1.8$ to 3.0.

Photoelectron escape probably does not decrease the heating rate in the adiabatic expansion scenario. As the clouds expand, they become less dense and thus the recombination rates decrease, increasing the ionization fraction in the clouds. As the electron column density increases, the photoelectrons are more easily trapped inside the cloud. Thus if the Pettini et al. (1990) results are correct even more questions about the clouds arise. What is their formation process? Are they confined? If they are not, what mass source accounts for their replacement since high-pressure clouds rapidly dissipate by thermal expansion? Can adiabatic cooling of low-pressure clouds explain the data? We explore some of these questions in a later paper (Shull & Donahue 1992).

For the metal-line systems, one can begin to constrain $U$ by observations of absorption lines of C III and C IV. We have rederived metallicity limits for two systems with observational detections or upper limits on C II, C III, C IV, and Si III or Si IV column densities. Our model incorporates the most recent calculations of photoionization cross sections from the Opacity Project. Although these cross sections are believed to be accurate to 10%, the ionization calculations also depend on accurate values of recombination and charge exchange rate coefficients of metal ions with H I and He I. The next advance in photoionization models will require these rate coefficients to an accuracy equivalent to the photoionization cross sections. Until this is done, inferences about the spectral shape of the intergalactic ionizing radiation field must be regarded with some suspicion.

This work was supported by the NASA Astrophysical Theory Program at Colorado (grant NAGW-766) and by a NASA Graduate Researchers Fellowship (M. D.). We are grateful to Max Pettini for sharing his results on narrow QSO absorption lines prior to publication. We thank Mark Voit for the idea to explore photoelectron escape from the clouds and acknowledge useful discussions with J. Black, R. Duncan, G. Ferland, T. Kallman, J. P. Ostriker, and E. Vishniac. The CNO and Si photoionization cross sections were computed by the U.S.–U.K. Opacity Project, supported in part by the NASA Astrophysical Theory Program at Colorado. We thank the members of this consortium, particularly Michael Seaton and Anil Pradhan, for permission to use these data prior to publication. Finally, we thank the referee for some astute comments about the consistent use of the Opacity Project data.

## APPENDIX

## PHOTOIONIZATION OF IRON

For the photoionization of iron by X-rays one must take into account the Auger electrons produced by photoionization of the inner shells, since as many as nine electrons (one photoelectron and eight Auger electrons) can be released from the atom as a result of a single K-shell photoionization event. We used the results of Jacobs & Rozsnyai (1986) to calculate the probability of $N_A$ Auger electrons following the ionization of a given subshell. These probabilities take into account the probabilities of radiative transitions and Coster-Kronig transitions.

In this section we use the convention that an Auger electron can be designated by an abbreviated notation, e.g., $KL_1L_{23}$. In this notation the first letter designates the quantum level $(n, l)$ from which the photoelectron was ejected ($K = 1s$; $L = 2s, 2p$; $M = 3s, 3p, 3d$; etc.). The second letter denotes the level from which the intermediate electron dropped in order to fill the hole left by the

photoelectron, and the third letter denotes the level from which the Auger electron was ejected. The subscripts are a shorthand for the convention of labeling the orbitals, such that "1" corresponds to the $s$ orbital, "23" corresponds to the $p$ orbitals ($^2P_{1/2}$, $^2P_{3/2}$), and "45" corresponds to the $d$ orbitals ($^2D_{3/2}$, $^2D_{5/2}$).

Weisheit & Dalgarno (1972) and Weisheit (1974) calculated the effective photoionization rate for elements with nuclear charge $Z \leq 10$ and $11 \leq Z \leq 18$, respectively. We can extend this formalism to iron ($Z = 26$). The effective photoionization rate, $\Gamma_{\rm eff}$, from ion stage $z$ for pure photoionization (no collisions), is defined by the ratio of ion populations in successive ion stages, $z$ and $z + 1$,

$$n_z \Gamma_z^{\rm eff} = n_e n_{z+1} \alpha_z , \tag{14}$$

where $n_e$ is the electron density and $\alpha_z$ is the rate coefficient for recombination from ion stage $z + 1$ to stage $z$. Here, $z = 1$ refers to neutral iron. In the following equations $\Gamma_z$ is defined as

$$\Gamma_z = \Gamma_{1s}(z) + \Gamma_{2s}(z) + \Gamma_{2p}(z) + \Gamma_{3s}(z) + \Gamma_{3p}(z) + \Gamma_{3d}(z) + \Gamma_{4s}(z) + n_e C_z , \tag{15}$$

where $\Gamma_{nl}(z)$ is the photoionization rate of the subshell ($nl$) of ion stage $z$ of Fe (Reilman & Manson 1978, with a factor of 10 decrease in the cross sections for $2s$ states shown in their Fig. 2). Thus, $\Gamma_{1s}(1)$ corresponds to the photoionization rate of the $1s$ subshell of Fe I. $C_z$ is the electron-impact collisional ionization rate from ion stage $z$.

We calculate the effective ionization rate by the following prescription:

$$\begin{aligned}
\Gamma_z^{\rm eff} &= \Gamma_z , && z = 1 \\
&= \Gamma_z + n_e \alpha_{z-1}^{\rm eff} - \sum_{i=z-1}^{1} \left(\frac{n_i}{n_z}\right) \phi_i^{(z-i)} , && 2 \leq z \leq 10 \\
&= \Gamma_z + n_e \alpha_{z-1}^{\rm eff} - \sum_{i=z-1}^{z-9} \left(\frac{n_i}{n_z}\right) \phi_i^{(z-i)} , && 11 \leq z \leq 23 \\
&= \Gamma_z , && 24 \geq z \leq 26 ,
\end{aligned} \tag{16}$$

where $n_e$ is the electron density and $\alpha_z^{\rm eff}$ is the effective recombination rate from ion $z + 1$ to ion $z$, including charge exchange with neutral hydrogen. That is,

$$\alpha_z^{\rm eff} = \alpha_z + \frac{n({\rm H}^\circ)}{n_e} \gamma_z \tag{17}$$

where $\gamma_z$ is the rate coefficient for H° charge exchange with ion $z$.

The functions $\phi_z$ in equation (16) are defined as follows:

$$\phi_z^{(i)} = f_{1s}(i, z)\Gamma_{1s}(z) + f_{2s}(i, z)\Gamma_{2s}(z) + f_{2p}(i, z)\Gamma_{2p}(z) + f_{3s}(i, z)\Gamma_{3s}(z) + f_{3p}(i, z)\Gamma_{3p}(z) , \tag{18}$$

where $i$ is the number of Auger electrons emitted $f_{nl}(i, z)$ is the probability that, following a photoionization of Fe ion stage $z$ in subshell $nl$, one photoelectron and $i - 1$ Auger electrons are emitted.

By using the former equations and photoionization rates for all lower stages of ionization and subshells of Fe, one may compute the ionization balance of iron in the following equation:

$$n_z = \frac{n_{z+1} \Gamma_z^{\rm eff}}{n_e \alpha_z^{\rm eff}} . \tag{19}$$

To derive the electron heat production, we assume that, following the photoionization of a K-shell ($1s$) electron, a $KL_{23}L_{23}$ electron is expelled 2/3 of the time; the other one-third of the time, a Coster-Kronig transition occurs and both a $KL_1L_{23}$ electron and a $L_1L_{23}M$ electron are expelled. We then assumed that cascades, either subsequent to a K-shell ionization or other subshell ionizations, can only occur in jumps of a single level. This assumption if relaxed, would decrease the number of electrons released. Most of the energy available for heating is contained in the $KLL$ Auger electrons. We then calculate the number of Auger electrons produced and estimate their energies by using average values of shell levels from Reilman & Manson (1978).

## REFERENCES


Allison, A. C., & Dalgarno, A. 1970a, Atomic Data, 1, 91
———. 1970b, Atomic Data, 1, 289
Arnaud, M., & Rothenflug, R. 1985, A&AS, 60, 425
Badnell, N. R. 1988, J. Phys. B, 21, 749
Bajtlik, S., Duncan, R. C., & Ostriker, J. P. 1988, ApJ, 327, 570
Baliunas, S., & Butler, S. E. 1980, ApJ, 235, L45
Bechtold, J., Weymann, R. J., Lin, Z., & Malkan, M. A. 1987, ApJ, 315, 180
Bergeron, J., & Stasinska, G. 1986, A&A, 169, 1
Black, J. H. 1981, MNRAS, 197, 553
Blades, J. C., Hunstead, R. W., Murdoch, H. S., & Pettini, M. 1985, ApJ, 288, 580
Broad, J. T., & Reinhardt, W. P. 1976, Phys. Rev. A, 14, 2159
Butler, S. E., & Dalgarno, A. 1979, ApJ, 234, 765
———. 1980, ApJ, 241, 838
Butler, S. E., Heil, T. G., & Dalgarno, A. 1979, ApJ, 241, 442
Chaffee, F. H., Foltz, C. B., Bechtold, J., & Weymann, R. J. 1986, ApJ, 301, 116
Chaffee, F. H., Foltz, C. B., Roeser, H.-J., Weymann, R. J., & Latham, D. W. 1985, ApJ, 292, 362
Chapman, R. D., & Henry, R. J. W. 1972, ApJ, 173, 243
Chen, M. H., Craseman, B., Karim, Kh. R., & Mark, H. 1981, Phys. Rev. A, 24, 1845
Corbin, M. 1990, ApJ, 357, 346
Corrigan, S. J. B. 1965, J. Chem. Phys., 43, 4381
Dalgarno, A., Heil, T. G., & Butler, S. E. 1981, ApJ, 245, 793
Dalgarno, A., & Lepp, S. 1987, in IAU Symp. 120, Astrochemistry, ed. M. S. Vardya & S. P. Tarafdar (Dordrecht: Reidel), 109
Daltabuit, E., & Cox, D. P. 1972, ApJ, 177, 855
Duncan, R., Vishniac, E., & Ostriker, J. P. 1991, ApJ, 368, L1

Espey, B. R., Carswell, R. F., Bailey, J. A., Smith, M. G., & Ward, M. J. 1989, ApJ, 342, 666
Ferland, G. 1989, O.S.U. Internal Report, 89-001
Fernley, J. A., Taylor, K. T., & Seaton, M. J. 1987, J. Phys. B, 20, 6457
Field, G. B., & Steigman, G. 1971, ApJ, 166, 59
Foltz, C. B., Weymann, R. J., Roeser, H.-J., & Chaffee, F. H. 1984, ApJ, 281, L1
Gaetz, T. J., & Salpeter, E. E. 1983, ApJS, 52, 155
Gaskell, C. M. 1982, ApJ, 263, 79
Grevesse, N. 1984, Phys. Scripta, T8, 49
Guilbert, P. W., Fabian, A. C., & McCray, R. 1983, ApJ, 266, 466
Hogan, C. J. 1987, ApJ, 316, L59
Hutchings, J. 1976, ApJ, 205, 103
Jacobs, V. L., & Rozsnyai, B. F. 1986, Phys. Rev. A, 34, 216
Karpas, Z., Anacich, V., & Huntress, W. T. 1979, J. Chem. Phys., 70, 2877
Lepp, S., McCray, R., Shull, J. M., Woods, D. T., & Kallman, T. 1985, ApJ, 288, 58
Lepp, S., & Shull, J. M. 1983, ApJ, 270, 578
Luo, D., & Pradhan, A. K. 1989, J. Phys. B, 22, 3377
Mac Low, M.-M., & Shull, J. M. 1986, ApJ, 302, 585
Mathews, W. D., & Ferland, G. 1987, ApJ, 323, 456 (MF)
McCarroll, R., & Valiron, P. 1976, A&A, 53, 83
Miralda-Escudé, J., & Ostriker, J. P. 1990, ApJ, 350, 1
Morton, D. C., & Dinerstein, H. 1976, ApJ, 204, 1
Namioka, T. 1964, J. Chem. Phys., 40, 3154
Nussbaumer, H., & Storey, P. J. 1983, A&A, 126, 75
Osterbrock, D. G. 1989, Astrophysics of Gaseous Nebulae and Active Galactic Nuclei (Mill Valley: University Science Books).
Peach, G., Saraph, H. E., & Seaton, M. J. 1988, J. Phys. B, 21, 3669
Peart, B., Bennett, M. A., & Dolder, K. 1985, J. Phys. B, 18, L439
Pettini, M., Hunstead, R. W., Smith, L. J., & Mar, D. P. 1990, MNRAS, 246, 545
Pradhan, A. K. 1988, in AIP Conf. Proc. 168, Atomic Processes in Plasmas, ed. A. Hauer & A. L. Merts (New York: AIP), 59
Rees, M. J. 1986, MNRAS, 218, 25P
Reilman, R. F., & Manson, S. T. 1978, Phys. Rev. A, 18, 2124
Rybicki, G. B., & Lightman, A. P. 1979, Radiative Processes in Astrophysics (New York: Wiley-Interscience)
Sargent, W. L. W., Boksenberg, A., & Steidel, C. C. 1988, ApJS, 68, 539
Sargent, W. L. W., & Steidel, C. C. 1990, in Baryonic Dark Matter ed. D. Lynden-Bell & G. Gilmore (Dordrecht: Kluwer), 223
Sargent, W. L. W., Steidel, C. C., & Boksenberg, A. 1990, ApJ, 351, 364
Sargent, W. L. W., Young, P. J., Boksenberg, A., & Tytler, D. 1980, ApJS, 42, 41
Seaton, M. J. 1987, J. Phys. B., 20, 6363
Shull, J. M. 1979, ApJ, 234, 761
Shull, J. M., & Donahue, M. 1992, in preparation
Shull, J. M., & Van Steenberg, M. E. 1982, ApJS, 48, 95; erratum, 49, 351
———. 1985, ApJ, 298, 268
Steidel, C. C., & Sargent, W. L. W. 1989, ApJ, 343, L33
———. 1990, AJ, 99, 1693
Stephens, T. L., & Dalgarno, A. 1972, J. Quant. Spectros. Rad. Transf., 12, 569
Weedman, D. W. 1986, Quasar Astronomy (Cambridge: Cambridge Univ. Press)
Weinberg, S. 1972, Gravitation and Cosmology (New York: Wiley)
Weisheit, J. C. 1974, ApJ, 190, 735
Weisheit, J. C., & Dalgarno, A. 1972, Astrophys. Lett., 12, 103
Williger, G. M., Carswell, R. F., Webb, J. K., Boksenberg, A., & Smith, M. G. 1989, MNRAS, 237, 635
Wilkes, B. J., & Carswell, R. F. 1982, MNRAS, 201, 645
Wishart, A. W. 1979, MNRAS, 187, 59P
Wolfe, A. M. 1983, ApJ, 268, L1
Woods, D. T., Shull, J. M., & Sarazin, C. R. 1981, ApJ, 249, 399
Yu, Y., & Seaton, M. J. 1988, J. Phys. B, 20, 6409